Model-scale jet noise analysis with a single-point, frequency-domain nonlinearity indicator

Kyle G. Miller, and Kent L. Gee

Articles you may be interested in

Surface curvature effects on the tonal noise of a wall-mounted finite airfoil
The Journal of the Acoustical Society of America **143**, 3460 (2018); 10.1121/1.5040981

Mechanisms of active control of sound radiation from an opening with boundary installed secondary sources
The Journal of the Acoustical Society of America **143**, 3345 (2018); 10.1121/1.5040139

Acoustic scattering from a cylindrical shell with an internal rigid plate: Analysis and experiment
The Journal of the Acoustical Society of America **143**, 3332 (2018); 10.1121/1.5040469

Variability due to short-distance favorable sound propagation and its consequences for immission assessment
The Journal of the Acoustical Society of America **143**, 3406 (2018); 10.1121/1.5040483

A theoretical model of fuselage pressure levels due to fan tones radiated from the intake of an installed turbofan aero-engine
The Journal of the Acoustical Society of America **143**, 3394 (2018); 10.1121/1.5038263

Acoustically induced cavity cloud generated by air-gun arrays—Comparing video recordings and acoustic data to modeling
The Journal of the Acoustical Society of America **143**, 3383 (2018); 10.1121/1.5040490

Model-scale jet noise analysis with a single-point, frequency-domain nonlinearity indicator

Kyle G. Miller[a)] and Kent L. Gee

Department of Physics and Astronomy, Brigham Young University, Provo, Utah 84602, USA

A single-point, frequency-domain nonlinearity indicator is calculated and analyzed for noise from a model-scale jet at Mach 0.85, Mach 1.8, and Mach 2.0. The nonlinearity indicator, ν_N, has been previously derived from an ensemble-averaged, frequency-domain version of the generalized Burgers equation (GBE) from Reichman, Gee, Neilsen, and Miller [J. Acoust. Soc. Am. **139**, 2505–2513 (2016)]. The indicator gives the spatial rate of change due to nonlinear processes in sound pressure level (SPL) spectrum, and two other indicators from the GBE—ν_S and ν_α—give the same quantity due to geometric spreading and absorption, respectively. Trends with frequency, angle, distance, and jet condition—supported both by spectral analysis and by calculation of the GBE-derived indicators—reveal a concentration of nonlinear effects along radials close to the plume with large overall SPLs. The calculated indicators for nonlinearity and absorption effects far from the source combine to give the same decay predicted by nonlinear theory for monofrequency sources. Trends in the ν_N indicator are compared with trends observed for other indicators such as pressure-derivative skewness and bicoherence, revealing both the qualitative and quantitative advantages of the ν_N indicator.
© 2018 Acoustical Society of America. https://doi.org/10.1121/1.5041741

I. INTRODUCTION

The role of nonlinear propagation effects in the propagation of high-amplitude jet noise has been a topic of discussion for several decades and has been examined for jets of various scales. Laboratory-scale jets have been studied to examine cumulative nonlinear effects,[1–4] coalescence in the sound field,[5] dependence on Reynolds number,[6] pressure skewness and pressure-derivative skewness values,[7,8] as well as analysis with other nonlinearity metrics.[9,10] The nonlinear evolution[11] and annoyance[12] of legacy commercial transports have also been characterized using a normalized quadspectral nonlinearity indicator. Noise waveforms from military jets have been used both to characterize near-field shock formation[13,14] and to model far-field shock formation,[15–17] along with comparison of computationally predicted and experimentally measured data.[18,19] Launch vehicles such as rockets have been studied to determine their acoustic noise characteristics[20] and shock formation growth,[21] in addition to predicting the noise propagation using model equations.[22]

Although most of these studies point to the presence of far-field nonlinear propagation effects, quantifying the physical significance of these effects remains a challenge. Many studies have been qualitative, creating difficulty in comparing results across different experiments. The studies that have been quantitative often present differing conclusions. For example, studies of model-scale jets for the prior Mach-1.92 jet,[2] heated supersonic jet,[8] Mach-2.0 jet,[7,9] Mach-1.5 heated and unheated jets,[2] and Mach-3.0 unheated jet[1,3,5] differ significantly in their description both of the spatial regions where cumulative nonlinear effects cause waveform distortion as well as the cause of such distortions.

Two main approaches have been used to unify the various types of analyses and experiments. One approach is to develop an *ad hoc* metric (e.g., average steepening factor,[23] pressure derivative skewness,[7,13] bicoherence,[9] etc.) that responds to nonlinear propagation phenomenon, then to study the metric behavior for different cases. For example, the pressure-derivative skewness and wave steepening factor have been used in conjunction to identify nonlinear trends in military jet noise[24] and laboratory-scale jet noise.[1] However, such metrics do not carry inherent physical meaning, but are instead used only in hopes of finding a correlation with physical phenomena. The second approach is to directly use a model equation to characterize the nonlinear propagation. For example, comparisons can be made between well-defined linear propagation—assuming spherical spreading and atmospheric absorption—and actual propagation, revealing the important physical differences between the two.[2] However, such a comparison requires a balance of large propagation distances and large measurement bandwidth to accurately detect differences between linear and nonlinear processes. If measurements are not made in the far-field, then the assumptions of linear propagation may be invalid due to other compounding effects (e.g., frequency-dependent source location and directivity).[9]

The generalized Burgers equation (GBE) is another model equation which has been used extensively to characterize nonlinear propagation, and comparisons between computational propagation with the GBE and actual propagation have shown good agreement.[17,25] The effective Gol'dberg number, derived from the GBE, considers known or assumed source and medium conditions to determine the relative

a)Electronic mail: kglenmiller@gmail.com

importance of cumulative nonlinearity in propagation.[1,10] The GBE has also been used to determine local rates of spectral changes due to nonlinearity and other linear effects.[26–28] The local analysis stems from the use of the "Morfey-Howell" indicator,[11] which has been previously studied for connection to nonlinear effects.[1,2,29] Specifically, this paper builds on the work of Reichman *et al.*[26] and Miller *et al.*,[27] both of which lay the groundwork for using a local, frequency-dependent nonlinearity indicator derived from the GBE.

This paper uses a derived quadspectral nonlinearity indicator to directly compare the effects of nonlinear propagation in model-scale jet noise to those of geometric spreading and atmospheric absorption. From known medium and propagation conditions, three GBE-derived indicators are calculated from a waveform to give the local rate of change in sound pressure level (SPL) due to spreading, absorption, and nonlinearity, respectively. The dataset analyzed in this paper has been previously studied for cumulative nonlinear propagation effects with bicoherence analysis,[9] along with the calculation of pressure derivative skewness[7] and other quadspectral nonlinearity indicators.[30] The previous results provide a benchmark for understanding trends in the GBE-derived indicators used here, as well as a comparison which highlights the additional insight gained from using the GBE-derived indicators.

First, to provide context for the use of the GBE-derived indicators—see previous works[26–28]—the indicator values are calculated for a computationally propagated sinusoid with conditions and amplitude analogous to the model-scale jet noise experiment. Next, trends with frequency, angle, and distance are examined in the spectra of noise from a Mach-2.0 jet, followed by a nonlinearity analysis of the same jet. The Mach-2.0 jet noise is compared to noise from Mach-0.85 and Mach-1.8 jets. From the spectral analysis, transfer of energy to frequencies above the peak-frequency region is observed for the Mach-1.8 and Mach-2.0 cases at angles near the principal propagation radial. The nonlinearity analysis matches the findings from the spectral analysis, showing quantitatively the high-frequency nonlinear growth and the peak-frequency nonlinear decay at angles near the principal propagation radial. For measurements made farthest from the source, the separate effects of nonlinear growth and absorption losses combine to give an effective reduction in the decay due to linear absorption alone.

II. METHODOLOGY

A. Indicators from the spectral GBE

While seeking a model equation to describe the nonlinear evolution of the power spectral density (PSD) for acoustic pressure, Morfey and Howell[11] found that an ensemble-averaged form of the GBE included a spectral quantity that could be used as a nonlinearity indicator. The Morfey and Howell-derived Q/S is defined as

$$\frac{Q}{S} = \frac{Q_{pp^2}}{p_{\rm rms}S_{pp}} = \frac{{\rm Im}\left\{E\left[\mathcal{F}^*\{p(t)\}\mathcal{F}\{p^2(t)\}\right]\right\}}{p_{\rm rms}S_{pp}}, \quad (1)$$

where Q_{pp^2} is the imaginary part of the cross-spectral density (or quadspectral density) between the pressure and pressure-squared waveforms, $p_{\rm rms}$ is the root-mean-square (rms) pressure, and S_{pp} is the autospectral or PSD. In addition, E denotes expectation value and $\mathcal{F}$ denotes a Fourier transform. Because Q/S involves the quadspectral density between pressure and squared pressure, it reveals phase coupling between two different frequencies that occurs in nonlinear harmonic generation as a result of quadratic nonlinearity.[9,31] The Q/S indicator has been variously applied to military aircraft noise,[12,32,33] model-scale jet noise,[2,30,34] rocket noise,[21] plane-wave tube data,[30] and numerically propagated waveforms.[31]

While the Q/S indicator has been used in many qualitative nonlinearity analyses,[2,12,21,30–34] a quantitative interpretation requires an understanding of its magnitude relative to other propagation mechanisms. To this end, the Q/S metric is used here in conjunction with the other GBE terms. Though several forms of the GBE exist, e.g., arbitrary spreading, stratified medium, etc., the frequency-domain version of the GBE is used here in order to work with frequency-domain nonlinearity indicators. The spectral GBE has separate terms for the effects of geometric spreading, absorption, and nonlinearity, respectively,

$$\frac{\partial \tilde{p}}{\partial r} + \frac{m}{r}\tilde{p} + \alpha'\tilde{p} = \frac{i}{2}\frac{\beta}{\rho_0 c_0^3}\omega\tilde{q}, \quad (2)$$

where $\sim$ denotes a complex Fourier spectrum; r is the distance from the source; m takes on values of 0, 0.5, or 1 for planar, cylindrical, and spherical waves, respectively; α' is a combination of the linear attenuation and dispersion coefficients for progressive plane waves; β is the coefficient of nonlinearity; ρ_0 is the equilibrium density of the medium; c_0 is the equilibrium sound speed, and $\tilde{q}$ is the Fourier transform of $p^2(t)$. If Eq. (2) is ensemble averaged, it can then be manipulated to include the Q/S term as defined in Eq. (1). As such, an ensemble-averaged version of the frequency-domain GBE yields an expression for the change in SPL over distance[26]

$$\frac{\partial L_p}{\partial r} = -10\log_{10}(e) \times \left(\frac{2m}{r} + 2\alpha + \frac{\omega\beta p_{\rm rms}}{\rho_0 c_0^3}\frac{Q}{S}\right)$$
$$\equiv \nu_S + \nu_\alpha + \nu_N \equiv \nu, \quad (3)$$

where L_p is the SPL spectrum (in decibels), $10\log_{10}(e) \approx 4.34$, and $\alpha = \Re\{\alpha'\}$ is the linear absorption coefficient. In addition, the indicators listed on the right-hand side of Eq. (3), by observation, are defined as

$$\nu_S \equiv -10\log_{10}(e) \times \frac{2m}{r},$$
$$\nu_\alpha \equiv -10\log_{10}(e) \times 2\alpha,$$
$$\nu_N \equiv -10\log_{10}(e) \times \frac{\omega\beta p_{\rm rms}}{\rho_0 c_0^3}\frac{Q}{S}. \quad (4)$$

That is, Eq. (4) gives expressions as functions of frequency for the change in SPL spectrum over distance due to

Kyle G. Miller and Kent L. Gee

geometric spreading, absorption, and nonlinearity, respectively. When calculated and compared in conjunction, the three indicators quantitatively relate three separate effects, with each indicator carrying explicit physical meaning. Positive values of the quantities in Eq. (4) indicate growth and negative values indicate decay. Note that for the nonlinear term, ν_N, the sign convention is opposite that used for the Q/S indicator,[11,34] for which a positive value signifies a loss of energy at a particular frequency.

B. Sinusoid propagation analysis

Before analyzing experimental data with the ν_N indicator, analysis of a numerical test case is useful to determine general trends and expected behavior of the indicator. For a simple test case, an initially sinusoidal waveform with amplitude similar to the model-scale jet noise was numerically propagated in air using a hybrid time-frequency domain algorithm for the GBE.[35] Unlike the jet noise case, which exhibits range and frequency-dependent geometric spreading in the near field, spherical spreading ($m = 1$) was assumed at all distances. For ease of subsequent comparison, the distance was scaled with respect to a jet nozzle diameter (D_j)—equal to 3.5 cm—and the atmospheric conditions were taken to be the same as in the experiment discussed in Sec. III, with temperature at 22.9 °C, atmospheric pressure at 96.8 kPa, and relative humidity at 53%. In order to approximate the peak frequency and rms amplitude of the jet data at 10 D_j, the sinusoid frequency and amplitude at 1 D_j were set to 4 kHz and 22 kPa, respectively. Since use of the GBE assumes $kr \gg 1$, emphasis is placed on distances of 10 D_j and greater, for which $kr > 25$ for all frequencies in the sinusoid propagation. For accuracy in the calculations, a sampling frequency of 88 MHz was used with 2^{16} waveform samples.

The nonlinearly and linearly propagated waveforms at 75 D_j are compared in Fig. 1(a), with the linear wave including only spherical spreading and atmospheric absorption effects. Relative to linear propagation, significant wave steepening has occurred in the nonlinear wave, along with a slight amplitude decrease. In addition, atmospheric dispersion[36] is evident by the rounded peak of the nonlinear waveform. The evolution of the harmonic amplitudes with distance is shown in Fig. 1(b), where the delayed onset of the higher harmonics corresponding to nonlinear wave steepening is visible. The fundamental always decreases in amplitude, but each sequential harmonic reaches a maximum amplitude at a successively larger distance from the source.

The calculation of ν_S, ν_α, and ν_N from Eq. (4) are carried out using the distance, frequency, assumed atmospheric conditions, and numerically propagated waveform. The ν_S indicator for spherical spreading as a function of distance and the ν_α indicator as a function of frequency are shown in Fig. 2, with circles showing the harmonics of the fundamental frequency. A line showing the slope of classical thermoviscous absorption ($e^{-\alpha}$ with $\alpha \propto f^2$) is overlaid to show that for the modeled conditions, nitrogen and oxygen vibrational relaxation effects fall largely outside the 4–40 kHz bandwidth of interest. Note the logarithmic ordinate of logarithmic quantities, which serves to better observe the slopes of the absorption curves.
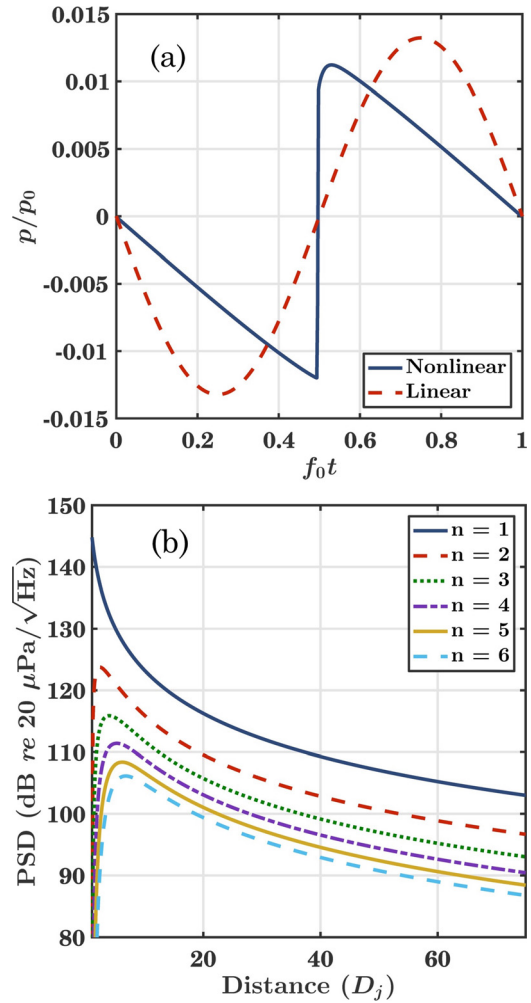

FIG. 1. (Color online) (a) Comparison of the nonlinearly and linearly propagated waveforms at 75 D_j. (b) Spectral amplitudes of the first six harmonics. Each sequential harmonic peaks at a successively larger distance from the source with the fundamental always decaying. The introduction of higher harmonic numbers corresponds to waveform steepening.

The similarity between high-frequency atmospheric and thermoviscous absorption trends is important in Sec. IV, where comparisons are made with analytical thermoviscous-medium behavior. As observed in Fig. 2, losses due to geometric spreading dominate absorption losses at all frequencies and distances, though past $\sim$40 D_j the effects of spreading and absorption are of similar magnitude for the higher harmonics.

The effects of spreading and absorption in Fig. 2 can be combined with the waveform-calculated ν_N to determine ν, the complete spatial rate of change in L_p as defined in Eq. (3). Then ν can be compared with the numerically calculated derivative of L_p, $\Delta L/\Delta D_j$, which is calculated for each harmonic from the curves in Fig. 1(b). Shown in Fig. 3 are the three indicators, their sum (ν), and $\Delta L/\Delta D_j$ as functions of distance. The error between ν and $\Delta L/\Delta D_j$ is less than 1% for all values shown. Very close to the source, ν_N is positive for each harmonic as the harmonics are initially generated. In fact, approaching 0 D_j (not pictured), the total indicator value approaches $\nu \to +\infty$. However, as shocks begin to form, energy is transferred from the low harmonics to even higher frequencies; this nonlinear energy transfer causes ν_N
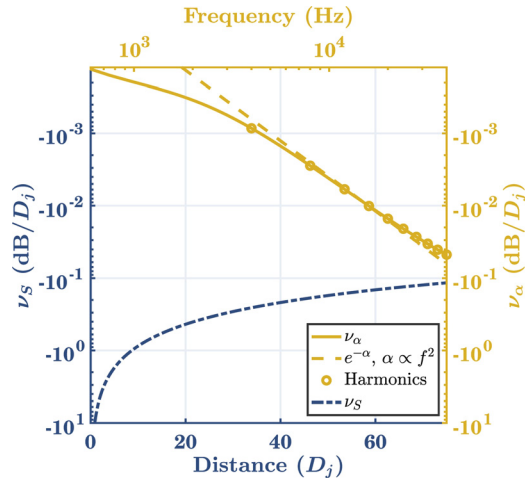
J. Acoust. Soc. Am. **143** (6), June 2018

Kyle G. Miller and Kent L. Gee   3481

FIG. 2. (Color online) Comparison of losses due to spherical spreading and atmospheric absorption. The ν_S indicator for spherical spreading ($m = 1$) is given as a function of distance, and the ν_α indicator—calculated from atmospheric conditions reported in the text—is given as a function of frequency. The dashed line shows the slope of classical thermoviscous absorption ($\alpha \propto f^2$), for which ν_α is closely aligned at the frequencies of interest (4–40 kHz). Circles indicate harmonics of the sinusoid, including the fundamental. Note that absorption losses are of similar magnitude as the spreading losses only for the high frequencies and far from the source.

to go negative for some of the lower harmonics, as seen in Fig. 3(b). For the tenth harmonic, ν_N decreases but remains positive away from the source. As pointed out by Blackstock,[37] the harmonic amplitudes of a nonlinear wave that undergoes unsteepening in the "old age" region decay more slowly than do harmonics of a linearly propagating wave. This difference is given by ν_N, which must therefore remain nonzero and positive out to very large distances. If the computational example is propagated to sufficient distance, ν_N becomes asymptotically positive for each harmonic other than the fundamental, which always remains negative. The asymptotic behavior of the ν_N indicator is explored in detail for the planar and diverging case by Miller et al.,[27] which corroborates the trends observed here.

In summary, the general behavior of the three indicators for this example is as follows: ν_S is independent of frequency and is generally large in magnitude compared to the effects of absorption and nonlinearity for the distances shown in Fig. 3. The ν_α indicator shows that absorption becomes increasingly negative with frequency, almost at the same rate as predicted by thermoviscous absorption for the frequencies of interest. The ν_N indicator is always negative for the fundamental frequency, indicative of energy loss from the peak region. For harmonics of the fundamental, ν_N is positive and infinite close to the source, then positive and small far from the source. The sign of ν_N at an intermediate distance from the source depends on the waveform amplitude, harmonic number, and atmospheric conditions. The trends explored in this section are useful for interpreting the analysis of the experimental model-scale data in subsequent sections.

III. MODEL-SCALE JET NOISE SPECTRAL ANALYSIS

This section examines the frequency content, directivity, spectra, and pressure-squared spectra of model-scale jet noise, followed by a comparison of jet conditions.
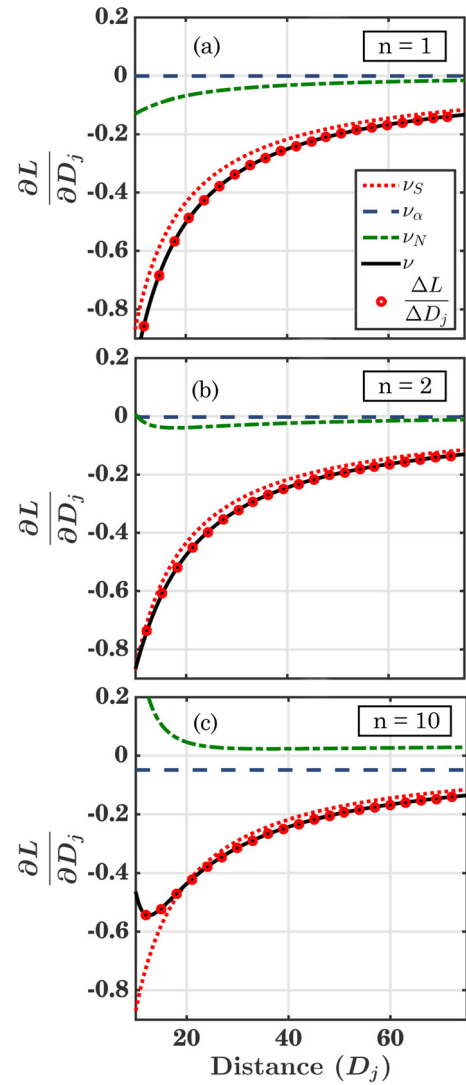

FIG. 3. (Color online) Comparison of the three indicators, their sum (ν), and the numerically calculated derivative of sound pressure level spectrum ($\Delta L/\Delta D_j$) for (a) the fundamental at 4 kHz, (b) the second harmonic at 8 kHz, and (c) the tenth harmonic at 40 kHz of the nonlinearly propagated waveform. Very close to the source ($<10\,D_j$, not pictured), harmonic strength is dominated by nonlinearity. Geometric spreading becomes the dominant effect at larger distances. For the tenth harmonic in (c), all three effects are of similar magnitude at $75\,D_j$.

A. Experiment description

The jet noise waveform data were taken at the National Center for Physical Acoustics' anechoic jet facility and have been previously reported and analyzed.[7,9,29,38] The measured jet conditions were subsonic Mach-0.85, overexpanded Mach-1.8, and ideally expanded Mach-2.0. Waveforms, sampled at 192 kHz, were acquired between 10 and 75 jet nozzle diameters ($D_j = 3.5$ cm) and between 80° and 150° (relative to upstream axis) in intervals of 5°, with a 3.18-mm and 6.35-mm microphone array whose origin was located $4\,D_j$ downstream of the nozzle exit. This origin is upstream from the expected overall noise source region,[39] but facility size constrained this positioning. Section IV contains additional detail on source location.

B. Mach-2.0 data

The experiment layout and overall sound pressure level (OASPL) for the ideally expanded Mach-2.0 jet condition can be observed in Fig. 4(a). Linear interpolation was used for this and subsequent figures to fill in values between measured data points. The measurement locations are represented by hollow circles and filled diamonds, with circles representing 3.18-mm microphones and diamonds representing 6.35-mm microphones. The OASPL map shows that the principal radiation radial occurs along 145°, or one set of microphones in from the edge nearest the jet flow. A peak frequency map created in the same fashion as Fig. 4(a) is shown in Fig. 4(b). The peak frequency was calculated by finding the geometric mean of the frequency range over which L_p was within 3 dB of the maximum level measured at a particular microphone. Figure 4(b) shows a general trend of high (low) peak frequencies in the near (far) field. In addition, a very high peak-frequency region is observed close to the source around ∼140° and projecting out to ∼40 D_j, and the lowest peak-frequency region is observed in the far field at 150°. This is due to the directivity and frequency-dependent source locations of the jet: lower frequencies are projected at angles closer to the jet flow axis[9] and high-frequency sources are generally located closer to the nozzle exit than low-frequency sources.[9,39] The combination of frequency-dependent source locations and directivities means that very close to the jet, the directivities at low and high frequencies remain distinct and have not overlapped.

This distinction accounts for the region of 9-kHz peak frequencies at 10 D_j, with the peak frequency values becoming nearly identical everywhere past 60 D_j as the directivities overlap. Section IV discusses the impact of source location on the nonlinear analysis.

The jet directivity can also be understood by examining SPL spatial maps at certain narrowband frequencies. Figure 5 shows the SPL for (a) 4 kHz, (b) 20 kHz, and (c) 40 kHz. A bin width of 187.5 Hz was used in the analysis. The directivity can be seen to change for each frequency, with higher frequencies radiating at shallower upstream angles (i.e., farther from the jet flow). In addition, the maximum level is seen to decrease for each higher frequency, which corresponds well with peak frequencies under 10 kHz. In Fig. 5(a), the low frequencies are seen to radiate at especially steep upstream angles, and perhaps the maximum radiation radial for this frequency is at an angle larger than 150°, i.e., too close to the jet
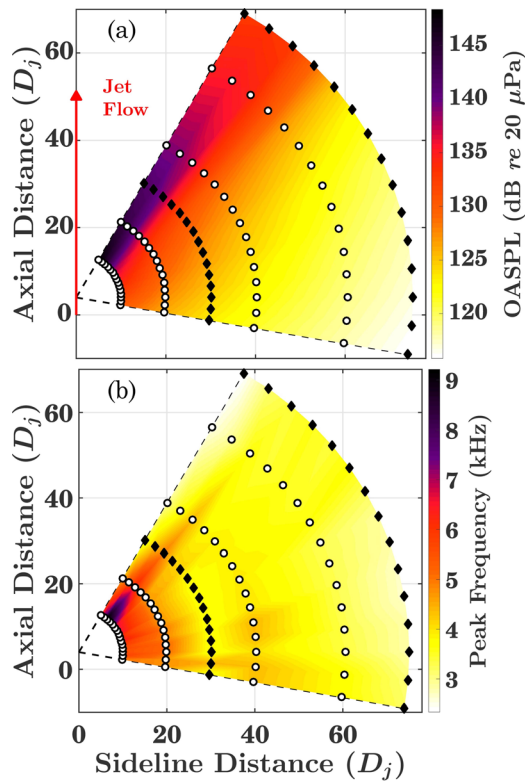

FIG. 4. (Color online) (a) OASPL and (b) peak frequency maps of the Mach-2.0 data. Color schemes were created using linear interpolation of data points. Data points are represented by hollow circles (3.18-mm mics) and filled diamonds (6.35-mm mics).
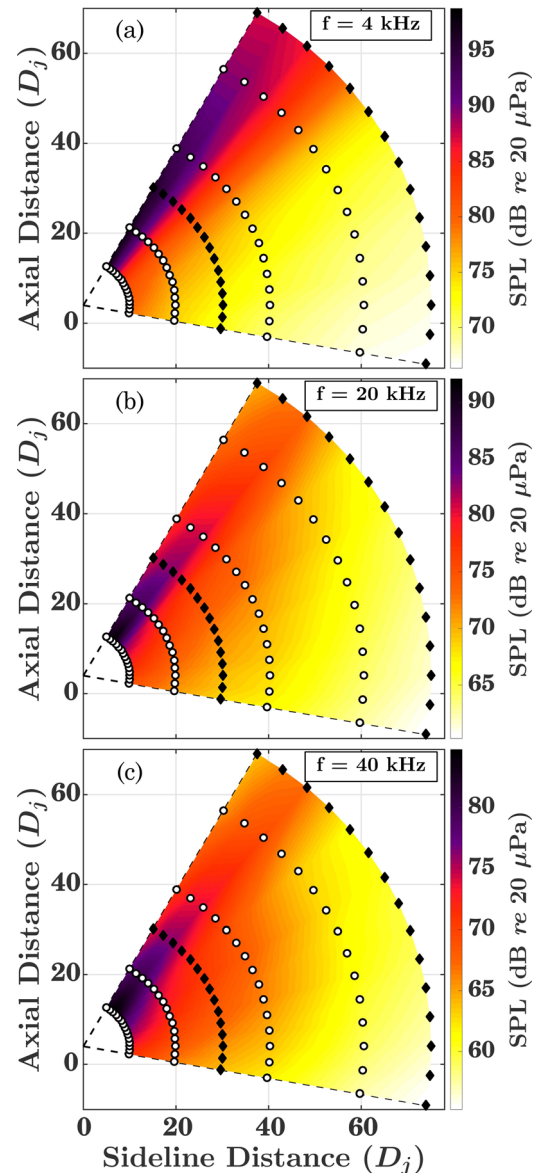

FIG. 5. (Color online) Narrowband SPL plots at three different frequencies. A bin width of 187.5 Hz was used to make these plots. The directivity changes for each plot, with lower frequencies radiating closer to the jet.

J. Acoust. Soc. Am. **143** (6), June 2018

Kyle G. Miller and Kent L. Gee   3483

to be captured by the microphones. To compare the jet noise to the propagated sinusoid in Sec. II, the difference between jet noise levels at 4 kHz and 20 kHz at 145° and 75 D_j is 15.1 dB, and the difference in levels between the fundamental and fifth harmonic of the sinusoid at 75 D_j is 14.6 dB, as seen in Fig. 1(b). The correspondence signifies a similar spectral shape between the two signals at this distance. At 75 D_j, the individual harmonic spectral density levels are about 8 dB higher for the initial sinusoid than for the experimental noise (along 145°) due to the broadband nature of the noise. In addition, the OASPL at 75 D_j is about 5 dB higher for the initial sinusoid than for the experimental noise (along 145°).

Other source characteristics are found by examining the PSD along a certain radial (arc) of constant angle (distance). Figure 6 shows PSDs along radials at (a) 135° and (b) 145°. A downward shift in peak frequency is observed along both radials in Fig. 6 due to the inner microphones being close to the geometric near field of a source with frequency-dependent source location, directivity, and spreading rate. It is important to note that this downward shift in peak frequency along a measurement radial is unrelated to nonlinear effects (see discussion regarding Fig. 4 of Ref. 9). For example, low-frequency noise is generated farther downstream from the

nozzle than is high-frequency noise,[39] so low- and high-frequency propagation radials differ—both from each other and from the microphone array—before converging at ~60 D_j. At 145° in Fig. 6(b), the frequency roll-off between 10 and 20 kHz changes from ~28 dB/octave at 10 D_j—close to expected 27.8 dB/octave decay rate for large-scale structure radiation[40]—to ~20 dB/octave at about 40 D_j—typical of shock-containing noise.[41] The high-frequency spectral shape remains fairly constant with distance after about 40 D_j, indicating that the energy losses due to absorption and energy gains due to nonlinearity are of similar magnitude; this is shown quantitatively in Sec. IV.

Changes in spectral shape and amplitude can be observed by viewing the spectra along an arc, as shown at 40 D_j in Fig. 7(a). As the angle approaches 145°—the principal radiation angle—the amplitude increases, but the spectra also become more peaked, with the $1/f^2$ high-frequency slope typical of supersonic jet noise becoming evident at 145°. Because the calculation of Q/S (and thus ν_N) requires computing the quadspectral density between the pressure and pressure squared waveforms, the PSDs of the waveform squared along the 40-D_j arc is also shown in Fig. 7(b). Irregularities such as nulls in the PSD of the squared
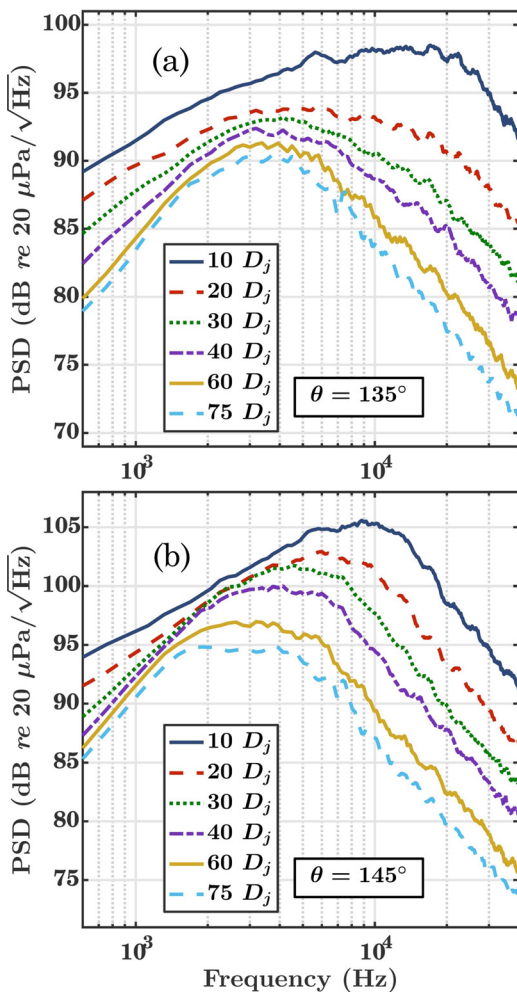

FIG. 6. (Color online) Measured spectra along radials at (a) 135° and (b) 145° for the Mach-2.0 data, showing the downward frequency shift. The principal radiation radial for this condition occurs along 145°.
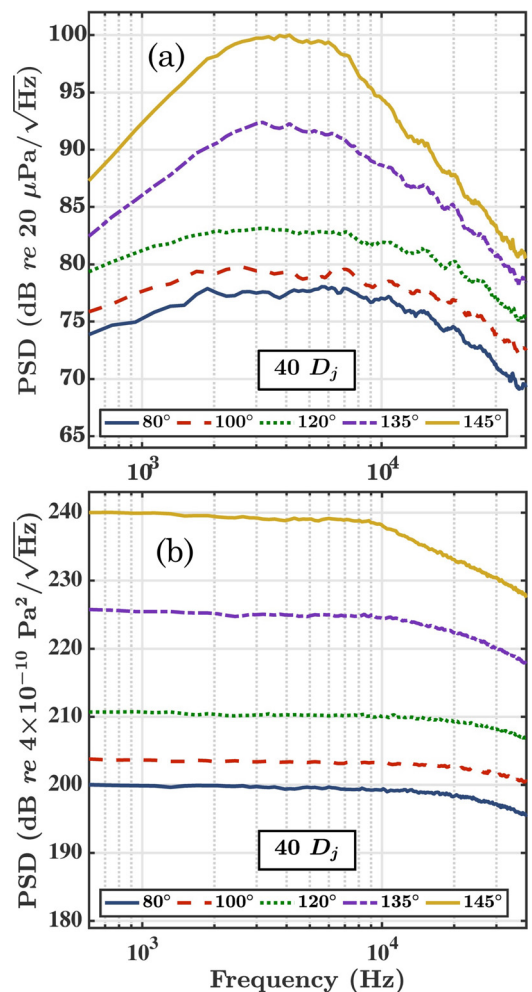
FIG. 7. (Color online) The PSDs of (a) the waveform and (b) the waveform squared from five microphones along an arc at 40 D_j. The PSDs of the waveform squared in (b) appear to be fairly smooth.

pressure can limit the predictive accuracy of ν_N,[42] but the PSDs in Fig. 7(b) appear to be fairly smooth and regular. Section IV describes additional details regarding accuracy of the ν_N calculation. The spectra for the other two jet conditions are briefly examined next.

C. Spectral comparison of jet conditions

In this section, spectral trends with jet Mach number are explored, building on previous characterizations of subsonic and supersonic jets.[43–45] The overexpanded Mach-1.8 and ideally expanded Mach-2.0 jet condition spectra are shown to be similar, whereas spectra for the subsonic Mach-0.85 jet condition behave differently in amplitude, peak frequency values, and high-frequency decay rate. The spectra along the maximum radiation radial of 150° is shown for both the (a) Mach-0.85 and (b) Mach-1.8 data in Fig. 8. In Fig. 8(a), the peak frequencies are nearly constant with distance and are seen to be lower than in Fig. 8(b). This is likely due to a low-frequency, compact noise source region located near the microphone array center (4 D_j from the nozzle exit) for the
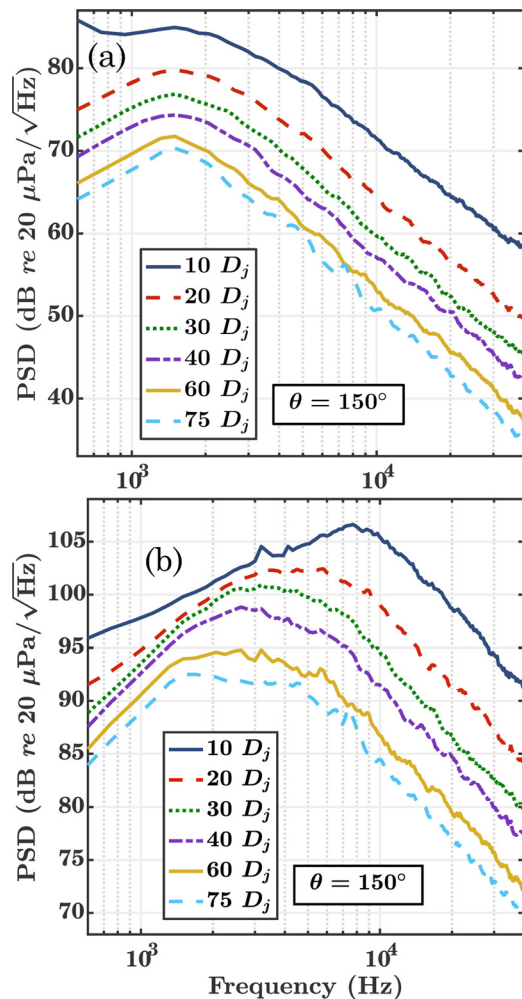

FIG. 8. (Color online) Measured spectra along 150° for the (a) Mach-0.85 and (b) Mach-1.8 data. The Mach-0.85 data observes a high-frequency spectral slope of about -27 dB/octave and constant peak frequency with distance. The Mach-1.8 data observes a high-frequency spectral slope of about -23 dB/octave and decreasing peak frequency with distance. The shallower slope results from a smaller overall spectral level.

Mach-0.85 condition,[39] with a low-frequency directivity that lines up with the 150° radial. The low-frequency source location and directivity are much different for the supersonic jets, as inferred from the peak-frequency shifts in Figs. 8(b) and 6.

The high-frequency spectral slopes are also different for the two jet conditions, a product of the different overall source strengths. The Mach-0.85 spectra in Fig. 8(a) have a high-frequency spectral roll-off of about $\sim$27 dB/octave, the decay rate for large-scale structure radiation.[39,40,46] The Mach-1.8 spectra in Fig. 8(b) have a much shallower high-frequency roll-off of about $\sim$23 dB/octave. The slope is steeper than the 20 dB/octave roll-off typical of acoustic shock-containing noise[41] and observed at Mach 2.0 in Fig. 6(b), but the decreased roll-off suggests some nonlinear generation of high frequencies at the Mach-1.8 jet condition. This shallow slope is roughly constant with distance after about 40 D_j, suggesting that significant nonlinear effects are occurring at distances closer than 40 D_j.

The model-scale jet serves as an extended source with frequency-dependent directivity evident in the noise spectra. Trends with distance show that the frequency-dependent directivity is more varied for high Mach numbers than for the low Mach number. Trends with angle show much higher levels close to the jet plume than at large angles; the peak radiation radial is 150° at Mach 0.85 and Mach 1.8 (or possibly greater than 150°, where we have no measurements), and 145° at Mach 2.0. The changes in peak frequency visible along some radials in the Mach-1.8 and Mach-2.0 jet condition spectra are likely products of the frequency-dependent directivity, while the shallow high-frequency roll-off results from nonlinear wave steepening. To further investigate the nonlinear behavior, the calculated indicator values from Eq. (4) are examined in the following section, along with a short discussion of the accuracy of the ν_N indicator.

IV. NONLINEARITY ANALYSIS

Nonlinear effects can be observed by analyzing trends in spectral slopes, such as those in Fig. 6. However, a more direct method of quantitatively observing nonlinearity from the spectra is to calculate the instantaneous change in sound pressure level spectrum, L_p, with distance due to nonlinearity. In addition, the strength of nonlinear effects can be directly compared with the effects of geometric spreading and atmospheric absorption. This quantitative nonlinear analysis is done through the use of the indicators ν_S, ν_α, and ν_N as defined in Eq. (4). The ν_N indicator is calculated and examined to find nonlinear trends with distance and angle. For the Mach-1.8 and Mach-2.0 jets, assuming spherical spreading is an oversimplification of the extended sources that could reduce the predictive accuracy of the ν_S indicator. Thus in this analysis, ν_S is only computed (assuming spherical spreading) to compare the predicted change in L_p with measured numerical derivatives as part of a rough benchmark of the ν indicator in Sec. IV A 3. The indicator values is compared with those found from the computationally propagated sinusoid in Sec. II B, and also to the strength of absorption calculated from ν_α.

Due to the high-amplitude, extended nature of the source with frequency-dependent directivity, low-frequency propagation radials close to the source differ markedly from the microphone measurement radials. Care must be taken when applying the models presented in Sec. II, which assume spherical spreading from a single point source for all frequencies. To properly interpret the ν_N calculations, two related conditions must be met. First, the GBE assumes $kr \gg 1$. Second, the propagation radials should be approximately parallel with the measurement radials, i.e., the frequency-dependent source location must appear close to the array origin of 4 D_j. In Fig. 7 of Gee et $al.$,[47] the frequency-dependent source locations of a Mach-1.8, ideally expanded jet with frequency-to-Strouhal number scaling of 24.44 kHz are shown. The peak-frequency source locations of the Mach-1.8 jet are similar to those of the Mach-1.9 jet studied by Tam et $al.$,[39] and are used to draw comparisons with the Mach-2.0 jet in this work. The source location for the Mach-1.8 jet from Ref. 47 is 4 D_j at ~15 kHz. Given that the frequency-to-Strouhal number scaling for the Mach-2.0 jet in this paper is 14.8 kHz, the corresponding frequency with a 4–D_j source location for this experiment is ~9 kHz. Extrapolating the results from Fig. 7 of Ref. 47 to 1 kHz (corresponding to ~600 Hz for this Mach-2.0 jet) gives a source location of about 17 D_j. Given these apparent source locations, we place a lower limit on valid frequencies for nonlinear analysis at 9 kHz for 10 D_j. and 600 Hz for 75 D_j, respectively. Data shown for intermediate distances have a low-frequency limit varying between 9 kHz and 600 Hz, with $kr > 29$ for all data shown in this section.

We place an upper frequency limit on valid frequencies for nonlinear analysis at 40 kHz—about 25% of the sampling frequency—where we expect the calculation of Q_{pp^2} in Eq. (1) to be accurate[42] based on the doubling of frequency components due to the waveform squaring and relationship with the Nyquist frequency.

A. Mach-2.0 data

1. Trends with distance and angle

The Mach-2.0 jet exhibits frequency-dependent source locations and directivities, which are evidenced by the spectra along propagation radials and arcs (see Figs. 6 and 7). However, past 60 D_j, the peak frequency appears to remain fairly constant. Nonlinear processes are evident in Fig. 6(b) from the constant high-frequency spectral slope along 145° and after about 40 D_j. The changes in peak frequency and spectral slope observed in the PSDs can be correlated with values of the ν_N indicator along the same radials. Figure 9 shows the calculated ν_N indicator along radials at (a) 135° and (b) 145°, with negative and positive values of ν_N indicating losses and gains in energy, respectively. Along 135°, the peak frequency ranges from 3.4 to 8.9 kHz. However, the frequency at which ν_N is most negative—signifying the largest nonlinear reduction in energy to generate higher frequencies—ranges from about 8.8 to 28 kHz. Similarly, the peak frequencies along the 145° radial range from 2.9 to 7.5 kHz, and the most negative value of ν_N ranges from about 7.9 to 15 kHz. The bulk of the energy required for nonlinear
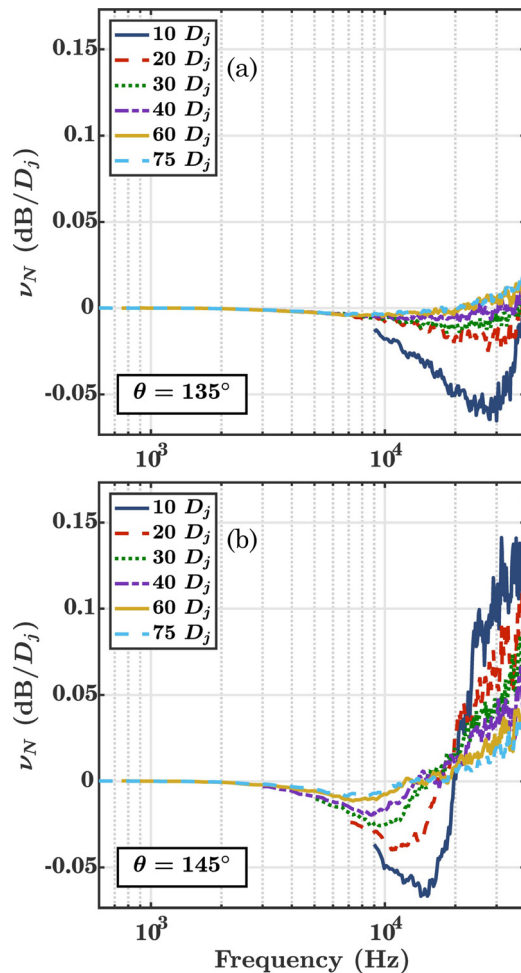

FIG. 9. (Color online) The ν_N indicator values for radials along (a) 135° and (b) 145°. The frequency where ν_N transitions from negative to positive decreases with distance, tracking the downward shift in peak frequency seen in Fig. 6. In addition, the same transition frequency is overall higher along 135° than for 145°, matching the higher peak frequencies along 135° as seen from Figs. 4(b) and 6. To uphold model assumptions based on estimated frequency-dependent source locations, only certain frequencies are shown.

harmonic generation is coming from frequencies appreciably higher than the PSD peak frequencies. This also reflects the factor of ω in the ν_N calculation shown in Eq. (4), where the multiplication of amplitude and frequency partially determine the nonlinear "cascading" in the formation of a $1/f^2$ slope.

Since nonlinear processes are dependent on both frequency and amplitude, spectral peak frequency shifts also change the frequency region where nonlinear effects are the largest. Visible at both angles in Fig. 9 is a transition from nonlinear loss to nonlinear gain in energy. The frequency at which this occurs decreases with distance along both radials, tracking the downward shift in peak frequency from the PSDs in Fig. 6. In addition, the frequency at which ν_N changes from negative to positive occurs at much higher frequencies along 135° in Fig. 9(a) than along 145° in Fig. 9(b). This matches the overall higher peak frequencies along 135° compared to 145°, as seen from Figs. 4(b) and 6. The downward shift along both radials and the higher transition frequencies along the 135° radial indicate that the general region of the spectrum with greatest amplitude at a given

location drives nonlinear energy transfer to higher frequencies. Similarly, Sec. II B showed that the harmonic of greatest amplitude for the sinusoidal case—the fundamental—continually drives nonlinear harmonic generation, i.e., ν_N is always negative for the fundamental. In addition, along the principal radiation radial in Fig. 9(b), the energy loss rate ($\sim$−0.01 to −0.05 dB/D_j) at 10 kHz and gain rate at 40 kHz ($\sim$+0.03 to +0.1 dB/D_j) for the experimental data are very similar in magnitude to the ν_N values for the second harmonic ($\sim$−0.01 to −0.04 dB/D_j) and tenth harmonic ($\sim$+0.03 to +0.11 dB/D_j) of the initial sinusoid between 15 and 75 D_j, as seen in Figs. 3(b) and 3(c).

The relative strength of nonlinearity along the various radials can be observed by viewing ν_N along an arc at a fixed distance. Figure 10 shows ν_N along five different radials, with the magnitude of the indicator increasing with angle. Though nonlinear processes are observed along both the 135° and 145° radials in Fig. 9, Fig. 10 shows that the nonlinear processes along the 145° radial are greater than twice the strength than those along the 135° radial. In addition, ν_N transitions from negative to positive at a much lower frequency along the 145° radial, corresponding to a lower peak along that radial.

The nonlinear growth and decay can be seen across all microphones through spatial maps of the ν_N indicator. The ν_N spatial maps are shown for various frequencies in Fig. 11, with data omitted within 40 D_j in Fig. 11(a) to uphold the model assumptions in Sec. II. The frequencies were chosen to show the indicator values for frequencies near the peak frequency, near the transition frequency where ν_N changes from negative to positive, and at high frequencies where significant nonlinear growth occurs. At low frequencies, such as in Fig. 11(a), energy is being lost due to nonlinearity at all locations. However, the loss is only significant between about 135° and 150°. At more shallow angles, not enough acoustic energy is available to drive nonlinear generation of higher frequencies. In fact, nonlinear effects are confined to angles between about 135° and 150° in each plot in Fig. 11. Similarly, Fig. 1 of Ref. 7 shows that the pressure derivative skewness values for the same Mach-2.0 dataset are only
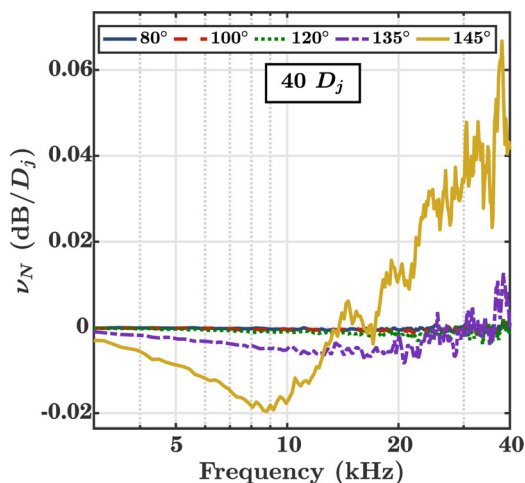

FIG. 11. (Color online) Spatial maps of ν_N for various frequencies. The frequencies were chosen to show ν_N values for frequencies near the peak frequency, near the transition frequency where ν_N changes from negative to positive, and at high frequencies where significant nonlinear growth occurs. Data are omitted within 40 D_j in (a) to uphold model assumptions.

FIG. 10. (Color online) The ν_N indicator values for various angles along an arc of 40 D_j. The nonlinearity increases significantly with angle.
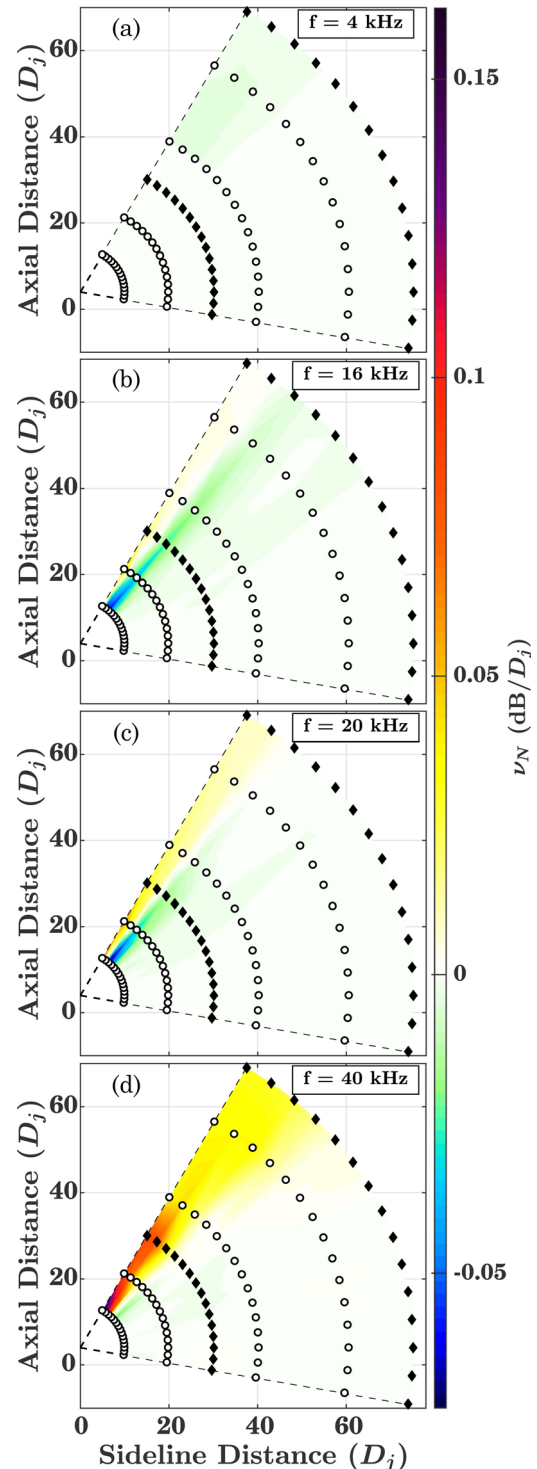
significantly above zero at the same angles. In addition, the bicoherence for the same dataset along 60 D_j, shown in Fig. 3 of Ref. 9, reveals no quadratic phase coupling (QPC), some QPC, and significant QPC at angles of 120°, 135°, and 150°, respectively. The trends from the calculated ν_N indicator agree well with trends from the pressure derivative skewness and bicoherence calculations.

In Figs. [11(b)] and [11(c)] of this paper, ν_N is seen to spatially transition from positive to negative with decreasing angle. The change from nonlinear growth to nonlinear decay tracks the overall transition from low to high peak frequency with decreasing angle—as seen in Fig. [4(b)]—with low peak frequencies corresponding to nonlinear growth at relatively low frequencies ($\sim$16 kHz). In Fig. [11(d)], the frequency is high enough that nonlinear growth occurs at all locations. The only exception is very close to the source, where ν_N is slightly negative due to a very high peak frequency in that region, as seen in Fig. [4(b)]. The ν_N indicator serves not only to show the presence of nonlinearity, but it also shows whether the transfer of energy is positive or negative at a particular frequency, giving insight into the nonlinear processes occurring based on peak frequency.

2. Nonlinearity and absorption

One specific benefit of the ν_N indicator is that it allows for the direct comparison of the effects of absorption and nonlinearity. The spectra in Fig. [6(b)] appear to preserve a constant high-frequency slope, even though the overall amplitude is decreasing due to spreading. In order to compare the high-frequency effects of absorption and nonlinearity without including spreading, the sum $\nu_N + \nu_\alpha$ is calculated. The sum is shown along 145°, the principal radiation radial for Mach 2.0, in Fig. [12]. Note that the sum appears to be about zero above 20 kHz at 40 D_j, the distance where the high-frequency spectral slopes in Fig. [6(a)] appear to remain constant. The trend indicates that overall growth has ceased for frequencies of 20–40 kHz past 40 D_j. To the contrary, pressure-derivative skewness analysis from the same dataset seen in Fig. 1 of Ref. [7] show increasing derivative skewness values out to 75 D_j, indicating continued shock growth at the farthest measurement distance. Similar pressure-derivative skewness results are seen from a Mach-3.0 jet observed by Baars *et al.*,[1] where the derivative skewness values peak at about 145 D_j. It is possible that the Mach-2.0 waveform shocks are still

strengthening at 75 D_j, but that the nonlinear harmonic growth is visible in the ν_N values for frequencies above 40 kHz. Conducting this analysis would require measurements at farther distances and with a greater sampling frequency than was possible in this experiment.

Despite the somewhat contrasting trends from the ν_N indicator and derivative skewness, important far-field behavior for the measured frequencies can be drawn from the ν_N calculations. In Fig. [12], the 75–D_j curve appears to converge to a line with linear exponential decay ($e^{-\alpha}$ with $\alpha \propto f$). The ν_α curve as defined in Eq. [(4)] is also plotted for comparison. As shown in Fig. [2], the slope of ν_α above about 4 kHz closely follows a quadratic exponential decay ($e^{-\alpha}$ with $\alpha \propto f^2$), typical of thermoviscous absorption. For initially sinusoidal nonlinear waveforms in the old-age region ($\alpha r \gg 1$), the asymptotic decay of the nth harmonic due to absorption for both plane waves and spherically diverging waves in a thermoviscous medium goes as $e^{-n\alpha_0 r}$—a linear exponential decay.[37] It is not surprising that a linear exponential decay is reached for noise waveforms as well. However, the asymptotic decay appears to be reached much more quickly for noise than for initial sinusoids. For example, at 75 D_j in Fig. [12], the rate of change appears to observe a linear exponential decay rate for some frequencies. Assuming a peak frequency of 4 kHz at 75 D_j and atmospheric absorption gives $\alpha_0 r \approx 7.2 \times 10^{-3}$, which is far from the old-age region for initial sinusoids (which occurs at more than 100 times this distance for the sinusoid discussed in Sec. [II B]). Previous work shows that shocks occur more quickly for noise waveforms than for sinusoids,[48] but more work is required to determine the behavior of the ν indicators near the onset of the old-age region for spherically spreading noise waveforms–including analysis at higher frequencies and larger distances from the source.

3. Indicator accuracy

To determine the accuracy of the ν_N calculation, which gives the predicted change in the sound pressure level spectrum, L_p, over distance, the indicator is compared against numerical derivatives of L_p. However, the minimum spacing between microphones is 10 D_j, so the spatial derivatives are approximate. Near-field effects from frequency-dependent source locations and directivities cause changes in L_p not predicted by ν_N, as discussed at the beginning of this section. In addition, spectral changes at large distances, such as those seen from 60 to 75 D_j in Fig. [6], are only a few decibels large—on the order of the spectral noisiness. Nonetheless, such a comparison provides a qualitative benchmark verification of the indicator.

The ν_N indicator gives an instantaneous derivative of L_p, whereas numerical derivatives taken between microphones are a centered-difference. Figure [13] compares the predicted change in sound pressure level—ν, or the sum $\nu_S + \nu_\alpha + \nu_N$—with numerical spatial derivatives of the PSD levels between microphones. A bin width of 3 kHz was used for this analysis to better observe the general trends. The numerical derivative, $\Delta L_p/\Delta r$, in Fig. [13] is a centered-difference between spectra taken by microphones at (a) 20 and 30 D_j and (b) 40 and 60 D_j. Since the ν values are instantaneous derivatives and the numerical derivative is centered between the microphones,
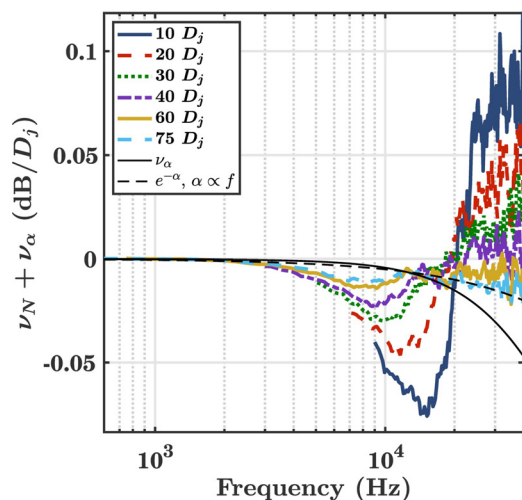

FIG. 12. (Color online) The sum $\nu_N + \nu_\alpha$ calculated along the 145° radial at Mach 2.0. The sum approaches zero at frequencies above about 20 kHz at 40 D_j. At 75 D_j, the sum for high frequencies converges to a slope of $e^{-\alpha}$ with $\alpha \propto f$—a linear exponential decay—rather than a slope with $\alpha \propto f^2$—a quadratic exponential decay, given approximately by ν_α as defined in Eq. [(4)].

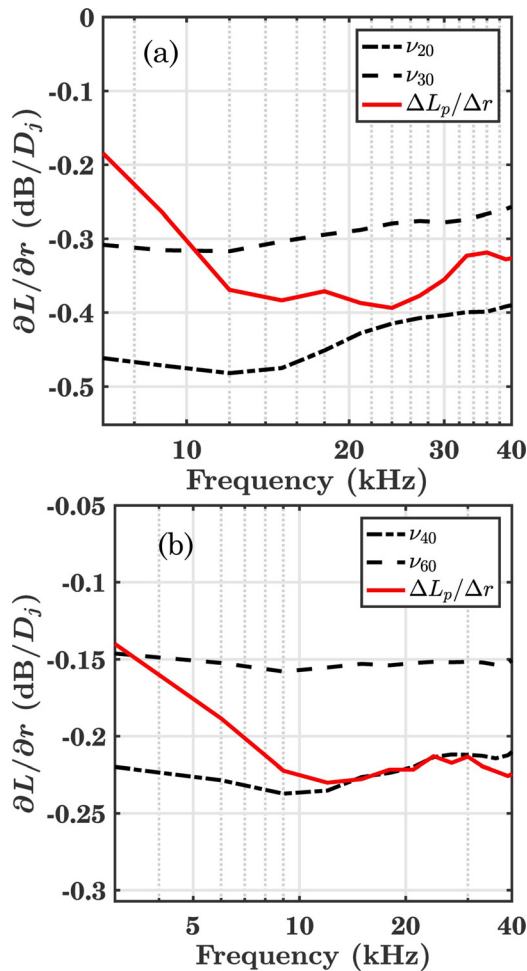Kyle G. Miller and Kent L. Gee

FIG. 13. (Color online) Predicted change in sound pressure level—ν, or the sum $\nu_S + \nu_\alpha + \nu_N$—with numerical derivatives of the PSD levels between microphones, $\Delta L_p/\Delta r$. The derivatives are taken along 145° at Mach 2.0 between (a) 20 and 30 D_j and (b) between 40 and 60 D_j. Some discrepancy is expected due to the extended, frequency-dependent nature of the source.

the red $\Delta L_p/\Delta r$ curve in each plot is expected to lie somewhere between the two black ν curves.

Though the estimated source location at 9 kHz is near the 4–D_j origin of the microphone array (see beginning of this section), there is a discrepancy at low frequencies in Fig. 13(a). This is most likely due to the frequency-dependent directivity of the source, especially evident in the near field,[9,39] as well as the large step size of the approximate spatial derivatives. In addition, spherical spreading is assumed for the ν_S metric, which may or may not be accurate for measurements near a model-scale jet.[5] However, from about 10 to 40 kHz in Fig. 13(a), the agreement between the predictions and actual derivatives is good, indicating that the lower limit of 7 kHz used at this distance is a reasonable estimate for the valid frequency range. The agreement is good across nearly all frequencies shown (lower limit of 3 kHz) between 40 and 60 D_j in Fig. 13(b), where the actual numerical derivative lies between the prediction from the ν_N indicator calculated at each distance.

B. Nonlinear comparison of jet conditions

The strength of nonlinear effects increases with waveform amplitude, and this section compares the nonlinearity

from data collected at Mach 0.85 and Mach 1.8 with the Mach-2.0 data. The OASPL is shown at (a) Mach 0.85 and (b) Mach 1.8 in Fig. 14. In Fig. 14(a), the levels are seen to be much smaller than for either the Mach-1.8 or Mach-2.0 cases, and negligible nonlinearity is expected in the data.[9] Note the secondary radiation lobe occurring in the Mach-1.8 data at about 125°, as seen in Fig. 14(b). This corresponds to a transition region from low to high peak frequency.[7]

Comparing the OASPL maps between the Mach-1.8 and Mach-2.0 data, the Mach-2.0 case only has values 2–4 dB higher than the Mach-1.8 case. The directivity has changed, with the main lobe being located more downstream at Mach 1.8. The ν_N values at 150° and 60 D_j are compared together for the three engine conditions in Fig. 15. As expected, negligible nonlinearity is observed for the Mach-0.85 case. The ν_N curve for this condition is extremely small in amplitude, with only noisy fluctuations. At the physical location discussed in Fig. 15, the OASPL level at Mach 2.0 is about 2 dB higher (factor of about 1.3) than at Mach 1.8. Similarly, the high-frequency ν_N values are about 1.25 as large at Mach 2.0 for each frequency, which agrees well with the difference in OASPL levels.

To examine the decay due to the effects of nonlinearity and absorption combined, the same plots as in Fig. 12 are shown for the (a) Mach-0.85 and (b) Mach-1.8 jet conditions in Fig. 16. The sum $\nu_N + \nu_\alpha$ is given at each distance, along with ν_α as defined in Eq. (4) (approximately a quadratic exponential decay of $e^{-\alpha}$ with $\alpha \propto f^2$) and a linear exponential decay ($e^{-\alpha}$ with $\alpha \propto f$). Each is along a 150° radial, which is the principal radiation radial for both conditions.
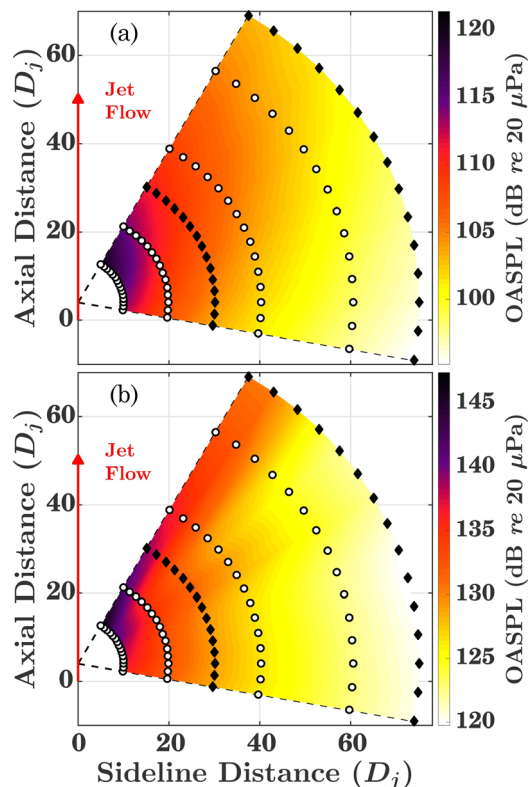

FIG. 14. (Color online) OASPL spatial maps of the (a) Mach-0.85 and (b) Mach-1.8 data. Note the much smaller levels in (a) and the secondary radiation lobe at about 125° in (b).
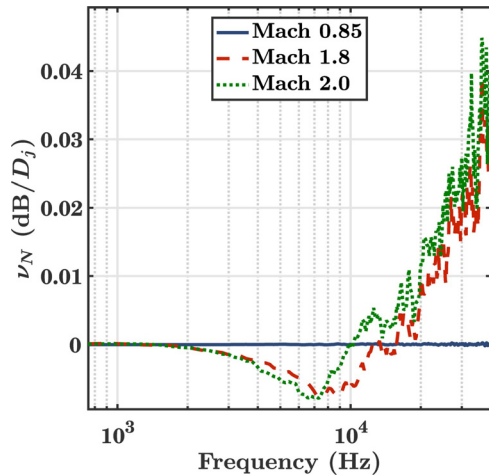
J. Acoust. Soc. Am. **143** (6), June 2018

Kyle G. Miller and Kent L. Gee   3489

FIG. 15. (Color online) The ν_N spectral values for three engine conditions at $150°$ and $60\ D_j$. The nonlinearity in the Mach-1.8 and Mach-2.0 data are comparable, whereas the nonlinearity for the Mach-0.85 data is negligible.

For the Mach-0.85 data, there is essentially no contribution to the sum from ν_N; the decay simply follows that of atmospheric absorption. For the Mach-1.8 data, however, the decay is similar to that of the Mach-2.0 data in Fig. 12: a linear exponential decay at $75\ D_j$.

In summary, as the jet condition increases, the OASPL increases and the directivity of the principal lobe moves upstream. Different from the other conditions, Mach 1.8 shows a secondary radiation lobe at about $125°$. The OASPL for Mach 0.85 is about $25\,dB$ less than Mach 1.8, which in turn is about $3\,dB$ less than Mach 2.0. The nonlinearity observed from the ν_N indicator is negligible at the lowest condition, and about 1.25 times as large at Mach 2.0 compared to Mach 1.8. The sum of the effects of absorption and nonlinearity produce a nearly quadratic exponential decay ($\alpha \propto f^2$) in the far field at Mach 0.85, but the far-field decay is that of a linear exponential ($\alpha \propto f$) for Mach 1.8 and Mach 2.0. (Note that ν_α was shown in Fig. 2 to decay with quadratic frequency dependence for frequencies above about 4 kHz.) The linear exponential decay at $75\ D_j$ for Mach 1.8 and Mach 2.0 shows that nonlinearity is significant enough for these two conditions to change the far-field nature of the waveforms. This confirms the expected results from theory[37] and from the calculations in Sec. II B, namely that a nonlinear waveform experiences a smaller decay in the far field than does a linear waveform. In fact, the far-field limit of the reduced absorption decay appears to be the same for initially sinusoidal waveforms as for noise waveforms, namely, a linear instead of quadratic exponential decay.

V. CONCLUSIONS

A quadspectral, frequency-domain nonlinearity indicator, ν_N, has been used to quantitatively yield the spatial rate of change in sound pressure level spectrum over distance for unheated, model-scale jet noise. The ν_N nonlinearity indicator gives a quantitative evaluation of nonlinearity from a single-point measurement, and comparison with the ν_S and ν_α indicators allows for direct comparison with spreading and absorption effects. Whereas nonlinearity is negligible
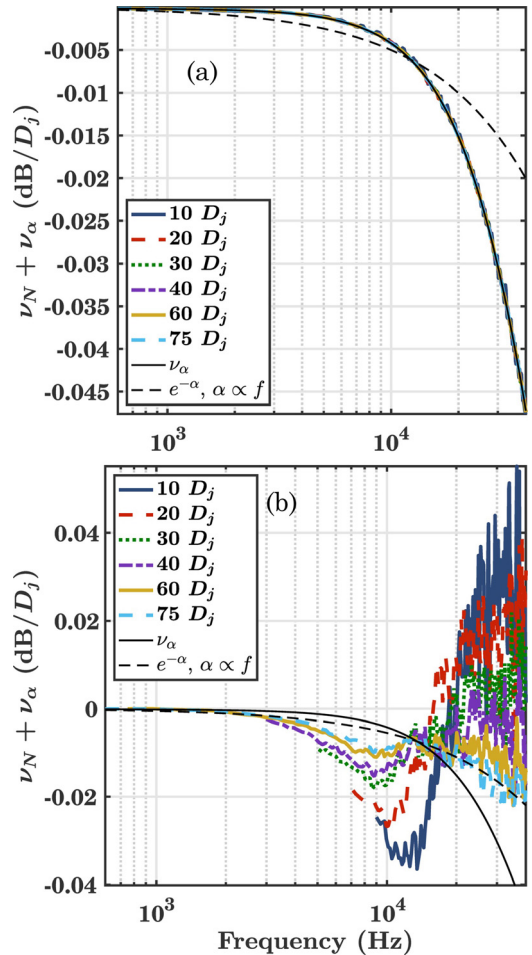

FIG. 16. (Color online) The sum $\nu_N + \nu_\alpha$ along $150°$ for (a) Mach 0.85 and (b) Mach 1.8. The contribution due to nonlinearity is essentially zero in (a), where the roll off follows that of absorption only (close to a quadratic exponential decay). For (b) Mach 1.8, the roll off approaches a linear exponential decay, similar to the Mach-2.0 case in Fig. 12. The linear exponential decay indicates a reduction in the expected absorption decay due to nonlinearity.

for the subsonic Mach 0.85 jet, nonlinear effects for the Mach 1.8 and Mach 2.0 jets are seen to be greater than or comparable with absorption along measured peak radiation radials, where the overall sound pressure level is greatest. This complements, and better quantifies, prior analyses involving the bicoherence and pressure derivative skewness.

Although the results represent a fully quantitative analysis of the effect of nonlinearity on jet noise spectral evolution, they also point to directions and the need for additional research. First, the geometric near-field—where the frequency-dependent source, spreading, and directivity effects are complex—needs to be more fully explored. Second, the noise waveforms appear to approach the old-age region relatively close to the source at only $75\ D_j$, where the effects of nonlinearity and absorption combine to cause a linear ($e^{-\alpha}$ with $\alpha \propto f$), rather than a quadratic ($e^{-\alpha}$ with $\alpha \propto f^2$) exponential decay. Additional research is needed to connect the frequency-domain nonlinearity analysis with time-domain nonlinearity indicators such as the derivative skewness, possibly with data taken at a higher sampling frequency and farther from the source. Finally, the old-age behavior and other quantitative

Kyle G. Miller and Kent L. Gee

insights presented here need to be investigated for supersonic jets of other scales and conditions.

ACKNOWLEDGMENTS

[1]W. J. Baars, C. E. Tinney, M. S. Wochner, and M. F. Hamilton, "On cumulative nonlinear acoustic waveform distortions from high-speed jets," J. Fluid Mech. 749, 331–366 (2014).

[2]B. P. Petitjean, K. Viswanathan, and D. K. McLaughlin, "Acoustic pressure waveforms measured in high speed jet noise experiencing nonlinear propagation," Int. J. Aeroacoust. 5, 193–215 (2006).

[3]W. J. Baars and C. E. Tinney, "Shock-structures in the acoustic field of a Mach 3 jet with crackle," J. Sound Vib. 333, 2539–2553 (2014).

[4]W. J. Baars, C. E. Tinney, and M. F. Hamilton, "Piecewise-spreading regime model for calculating effective Gol'dberg numbers for supersonic jet noise," AIAA J. 54, 2833–2842 (2016).

[5]R. Fiévet, C. E. Tinney, W. J. Baars, and M. F. Hamilton, "Coalescence in the sound field of a laboratory-scale supersonic jet," AIAA J. 54, 254–265 (2016).

[6]J. A. Gallagher and D. K. McLaughlin, "Experiments on the nonlinear characteristics of noise propagation from low and moderate Reynolds number supersonic jets," AIAA Paper 81-2041, (1981).

[7]K. L. Gee, T. B. Neilsen, and A. A. Atchley, "Skewness and shock formation in laboratory-scale supersonic jet data," J. Acoust. Soc. Am. 133, EL491–EL497 (2013).

[8]P. Mora, N. Heeb, J. Kastner, E. J. Gutmark, and K. Kailasanath, "Impact of heat on the pressure skewness and kurtosis in supersonic jets," AIAA J. 52, 777–787 (2014).

[9]K. L. Gee, A. A. Atchley, L. E. Falco, M. R. Shepherd, L. S. Ukeiley, B. J. Jansen, and J. M. Seiner, "Bicoherence analysis of model-scale jet noise," J. Acoust. Soc. Am. 128, EL211–EL216 (2010).

[10]M. F. Hamilton, "Effective Gol'dberg number for diverging waves," J. Acoust. Soc. Am. 140, 4419–4427 (2016).

[11]C. L. Morfey and G. P. Howell, "Nonlinear propagation of aircraft noise in the atmosphere," AIAA J. 19, 986–992 (1981).

[12]M. Downing, K. L. Gee, S. A. McInerny, T. B. Neilsen, and M. M. James, "Do recent findings on jet noise answer aspects of the Schultz curve?," Proc. Mtgs. Acoust. 19, 040022 (2013).

[13]K. L. Gee, T. B. Neilsen, J. M. Downing, M. M. James, R. L. McKinley, R. C. McKinley, and A. T. Wall, "Near-field shock formation in noise propagation from a high-power jet aircraft," J. Acoust. Soc. Am. 133, EL88–EL93 (2013).

[14]B. O. Reichman, J. M. Downing, A. Aubert, K. L. Gee, T. B. Neilsen, R. L. McKinley, A. T. Wall, and M. M. James, "Acoustical environment during F-35B vertical landing operations," J. Aircr. 53, 1975–1979 (2016).

[15]D. T. Blackstock, "Nonlinear propagation distortion of jet noise," in Proceedings of the Third Interagency Symposium on University Research in Transportation Noise, Salt Lake City, UT (November 12–14, 1975), pp. 389–397.

[16]H. H. Brouwer, "Numerical simulation of nonlinear jet noise propagation," AIAA Paper 2005-3088 (2005).

[17]B. Reichman, A. T. Wall, K. L. Gee, T. B. Neilsen, J. M. Downing, M. M. James, and R. L. McKinley, "Modeling far-field acoustical nonlinearity from F-35 aircraft during ground run-up," AIAA Paper 2016-1888 (2016).

[18]K. L. Gee, V. W. Sparrow, M. M. James, J. M. Downing, C. M. Hobbs, T. B. Gabrielson, and A. A. Atchley, "The role of nonlinear effects in the propagation of noise from high-power jet aircraft," J. Acoust. Soc. Am. 123, 4082–4093 (2008).

[19]S. Saxena, P. J. Morris, and K. Viswanathan, "Algorithm for the nonlinear propagation of broadband jet noise," AIAA J. 47, 186–194 (2009).

[20]J. N. Cole, R. T. England, and R. G. Powell, Effects of Various Exhaust Blast Deflectors on the Acoustic Noise Characteristics of 1,000 Pound-Thrust Rockets (Wright Air Development Division, Air Research and Development Command, United States Air Force, 1960).

[21]S. A. McInerny and S. M. Ölçmen, "High-intensity rocket noise: Nonlinear propagation, atmospheric absorption, and characterization," J. Acoust. Soc. Am. 117, 578–591 (2005).

[22]M. Muhlestein, K. L. Gee, T. B. Neilsen, and D. C. Thomas, "Prediction of nonlinear propagation of noise from a solid rocket motor," Proc. Mtgs. Acoust. 18, 040006 (2012).

[23]M. B. Muhlestein, K. L. Gee, T. B. Neilsen, and D. C. Thomas, "Evolution of the average steepening factor for nonlinearly propagating waves," J. Acoust. Soc. Am. 137, 640–650 (2015).

[24]K. L. Gee, T. B. Neilsen, D. C. Thomas, B. O. Reichman, M. Muhlestein, J. M. Downing, M. M. James, and R. L. McKinley, "Comparison of two time-domain measures of nonlinearity in near-field propagation of high-power jet noise," AIAA Paper 2014-3199 (2014).

[25]K. L. Gee, J. M. Downing, M. M. James, R. C. McKinley, R. L. McKinley, T. B. Neilsen, and A. T. Wall, "Nonlinear evolution of noise from a military jet aircraft during ground run-up," AIAA Paper 2012-2258 (2012).

[26]B. O. Reichman, K. L. Gee, T. B. Neilsen, and K. G. Miller, "Quantitative analysis of a frequency-domain nonlinearity indicator," J. Acoust. Soc. Am. 139, 2505–2513 (2016).

[27]K. G. Miller, K. L. Gee, and B. O. Reichman, "Asymptotic behavior of a frequency-domain nonlinearity indicator for solutions to the generalized Burgers equation," J. Acoust. Soc. Am. 140, EL522–EL527 (2016).

[28]K. G. Miller, B. O. Reichman, K. L. Gee, T. B. Neilsen, and A. A. Atchley, "Quantitative nonlinearity analysis of model-scale jet noise," AIP Conf. Proc. 1685, 090003 (2015).

[29]K. L. Gee, A. A. Atchley, L. E. Falco, and M. R. Shepherd, "Nonlinearity analysis of model-scale jet noise," AIP Conf. Proc. 1474, 307–310 (2012).

[30]L. E. Falco, "Single-point nonlinearity indicators for the propagation of high amplitude acoustic signals," Ph.D. thesis, The Pennsylvania State University, State College, PA, 2007.

[31]D. E. Gagnon, "Bispectral analysis of nonlinear acoustic propagation," Ph.D. thesis, The University of Texas at Austin, Austin, TX, 2011.

[32]K. L. Gee, T. B. Gabrielson, A. A. Atchley, and V. W. Sparrow, "Preliminary analysis of nonlinearity in military jet aircraft noise propagation," AIAA J. 43, 1398–1401 (2005).

[33]S. McInerny, K. L. Gee, M. Downing, and M. James, "Acoustical nonlinearities in aircraft flyover data," AIAA Paper 2007-3654 (2007).

[34]K. L. Gee, B. P. Petitjean, D. K. McLaughlin, and V. W. Sparrow, "Nonlinear propagation of noise radiated from supersonic jets," in Proceedings of Noise-Con 04, Baltimore, MD (July 12–14, 2004), pp. 725–733.

[35]K. L. Gee, "Prediction of nonlinear jet noise propagation," Ph.D. thesis, Pennsylvania State University, State College, PA, 2005.

[36]M. F. Hamilton, Y. A. Il'inskii, and E. A. Zabolotskaya, "Dispersion," in Nonlinear Acoustics (American Press, San Diego, CA, 1998), pp. 151–175.

[37]D. T. Blackstock, "Once nonlinear, always nonlinear," AIP Conf. Proc. 838, 601–606 (2006).

[38]K. L. Gee, M. R. Shepherd, L. E. Falco, A. A. Atchley, L. S. Ukeiley, B. J. Jansen, and J. M. Seiner, "Identification of nonlinear and near-field effects in jet noise using nonlinearity indicators," AIAA Paper 2007-3653 (2007).

[39]C. K. W. Tam, K. Viswanathan, K. K. Ahuja, and J. Panda, "The sources of jet noise: Experimental evidence," J. Fluid Mech. 615, 253–292 (2008).

[40]T. B. Neilsen, K. L. Gee, A. T. Wall, and M. M. James, "Similarity spectra analysis of high-performance jet aircraft noise," J. Acoust. Soc. Am. 133, 2116–2125 (2013).

[41]S. N. Gurbatov and O. V. Rudenko, "Statistical phenomena," in Nonlinear Acoustics (American Press, San Diego, CA, 1998), pp. 377–398.

[42]K. G. Miller, "Theoretical and experimental investigation of a quadspectral nonlinearity indicator," Master's thesis, Brigham Young University, Provo, UT, 2016.

[43]P. J. Morris, "A note on noise generation by large scale turbulent structures in subsonic and supersonic jets," Int. J. Aeroacoust. 8, 301–315 (2009).

[44]C. K. W. Tam, "On the noise of a nearly ideally expanded supersonic jet," J. Fluid Mech. 51, 69–95 (1972).

[45]K. Viswanathan, "Analysis of the two similarity components of turbulent mixing noise," AIAA J. 40, 1735–1744 (2002).

[46] C. K. W. Tam, M. Golebiowski, and J. M. Seiner, "On the two components of turbulent mixing noise from supersonic jets," AIAA Paper 96-1716 (1996).

[47] K. L. Gee, M. Akamine, K. Okamoto, T. B. Neilsen, S. Tsutsumi, S. Teramoto, T. Okunuki, and M. Cook, "Characterization of supersonic laboratory-scale jet noise with vector acoustic intensity," AIAA Paper 2017-3519 (2017).

[48] M. Muhlestein and K. Gee, "Experimental investigation of a characteristic shock formation distance in finite-amplitude noise propagation," Proc. Mtgs. Acoust. 12, 045002 (2011).